






Article

Analysis of the First Optical Detection of a Meteoroidal Impact on the Lunar Surface Recorded from Brazil

David Duarte Cavalcante Pinto ^{1,2,*} , Masahisa Yanagisawa ³, Marcelo Luiz do Prado Villarroel Zurita ^{4,5}, Romualdo Arthur Alencar Caldas ^{2,4}, Marcelo Domingues ^{4,6}, Rafaela Lisboa Costa ¹ , Rodrigo Lins da Rocha Júnior ¹, Fabrício Daniel dos Santos Silva ¹ , Heliofábio Barros Gomes ¹ , Helber Barros Gomes ¹, Maria Luciene Dias de Melo ¹, Lucas de Moraes Teixeira ^{2,7}, Ernande Roberto da Silva Júnior ², Neftali Dias Cavalcante Junior ^{2,8} and Dirceu Luís Herdies ⁹ 

- ¹ Institute of Atmospheric Sciences, Federal University of Alagoas, Maceió 57072-900, Brazil; rafaelalisboa@gmail.com (R.L.C.); rodrigo.junior@icat.ufal.br (R.L.d.R.J.); fabricio.santos@icat.ufal.br (F.D.d.S.S.); heliofabio@icat.ufal.br (H.B.G.); helber.gomes@icat.ufal.br (H.B.G.); maria.melo@icat.ufal.br (M.L.D.d.M.)
- ² Center of Astronomical Studies of Alagoas, Maceió 57051-090, Brazil; romualdo.caldas@hu.ufal.br (R.A.A.C.); lucas.teixeira@igdem.ufal.br (L.d.M.T.); ernande@visionline.com.br (E.R.d.S.J.); ndcj1@aluno.ifal.edu.br (N.D.C.J.)
- ³ Department of Engineering Science, The University of Electro-Communications, Tokyo 182-8585, Japan; yanagi@uec.ac.jp
- ⁴ Brazilian Meteor Observation Network, São Paulo 15190-000, Brazil; marcelo.zurita@bramonmeteor.org (M.L.d.P.V.Z.); marcelo@casb.com.br (M.D.)
- ⁵ Astronomy Association of Paraíba, João Pessoa 58039-100, Brazil
- ⁶ Clube de Astronomia de Brasília, Brasília 71070-714, Brazil
- ⁷ Institute of Geography, Development and Environment, Federal University of Alagoas, Maceió 57072-900, Brazil
- ⁸ Federal Institute of Alagoas, Maceió, 57020-600, Brazil
- ⁹ National Institute for Space Research, Cachoeira Paulista, São Paulo 12630-000, Brazil; dirceu.herdies@inpe.br
- * Correspondence: david.duarte@icat.ufal.br



Citation: Duarte Cavalcante Pinto, D.; Yanagisawa, M.; Zurita, M.L.d.P.V.; Caldas, R.A.A.; Domingues, M.; Costa, R.L.; da Rocha Júnior, R.L.; dos Santos Silva, F.D.; Barros Gomes, H.; Barros Gomes, H.; et al. Analysis of the First Optical Detection of a Meteoroidal Impact on the Lunar Surface Recorded from Brazil. *Remote Sens.* **2021**, *14*, 2974. <https://doi.org/10.3390/rs14132974>

Academic Editor: Akira Iwasaki

Received: 20 October 2021

Accepted: 28 November 2021

Published: 22 June 2022

Publisher's Note: MDPI stays neutral with regard to jurisdictional claims in published maps and institutional affiliations.



Copyright: © 2021 by the authors. Licensee MDPI, Basel, Switzerland. This article is an open access article distributed under the terms and conditions of the Creative Commons Attribution (CC BY) license (<https://creativecommons.org/licenses/by/4.0/>).

Abstract: Two lunar flashes are reported and fully analyzed, with one of them fulfilling every criterion preconized in the literature for the characterization of an impact, including confirmation by two simultaneous observations. It happened at 07:13:46 UT on 14 December 2017, at the selenographic coordinates of 9.79° ($\pm 0.06^\circ$)N and 45.42 ($\pm 0.07^\circ$)E. The peak magnitudes in the R and V bands vary from 6.3 to 7.9 and from 7.4 to 9.0, respectively, depending on the observatory, as the cameras' exposure times were considerably different. The impactor mass is estimated to be between 1.6 and 2.0 kg, with a diameter of 10 to 11 cm, having produced a crater of 8.4 to 8.9 m in diameter. Results for the second flash are also presented and discussed, although the confirmation of an impact was not possible due to a pause in the recordings at one of the sites. The observations took place as part of an inaugural observing campaign in Brazil for lunar impact flash (LIF) detection conceived by the Brazilian Meteor Observation Network (BRAMON) and were carried out by two teams located in different states in the Northeast Region of Brazil, about 353 km apart from each other, at a time when the Moon was crossing the densest part of the Geminid meteoroid stream in 2017. The observing setups included 0.13 m and 0.2 m telescopes, both equipped with sensitive cameras. The Maceió setup probably delivered the finest definition ever reported in the literature for lunar impact monitoring, resulting in high-accuracy positioning. This will certainly aid in finding the associated crater from orbiter images, which will substantiate another work, aimed at performing a comparative analysis between the results from our photometry and the data retrieved by the LRO images. These observations were also very likely the first and the only one so far made by a normal framerate camera and a long-exposure camera simultaneously. The associated benefits are commented on. The source of the impactors is also discussed. In view of the successful results of this experience, national observing campaigns of this kind will be given continuation.

Keywords: lunar remote sensing; optical detection; impact flashes; meteoroids; crater; instrumentation; monitoring; observing campaigns

1. Introduction

The surface of the Moon is often impacted by objects ranging in size from submicron dust to large comets and asteroids [1]. They collide with the lunar surface at velocities exceeding several kilometers per second [2]. This happens even to the smallest meteoroids that venture towards the Moon, given the absence of a dense atmosphere around its body. The impact speed largely depends on the source of the impactor, which varies considerably between the sporadic (background) population and the ones associated with a specific meteoroid stream [3]. For meteoroids of sporadic origin, early efforts have been made to ascertain their average speed, with an old NASA Technical Memorandum presenting the near-Earth value of 17 km/s [4]. The model developed by [5], on the other hand, proposed an average flux-weighted speed of 23.9 km/s, which the authors found to be congruent with observations. It is common in studies on lunar impact flashes (LIFs) to adopt one of the average values in that range for all events related to sporadic meteoroids, albeit the actual speed can vary from a minimum of 5 km/s to a maximum of 65 km/s [3]. As for the shower meteoroids, there is nearly no variation among impactors belonging to the same stream, but the difference between each stream can be pronounced, with Geminid meteoroids impacting the Moon at typically 32–34 km/s, the Perseids at 59 km/s, and the Leonids at 70 km/s [3].

When a meteoroid collides with the Moon, a transient luminous event, called an LIF, occurs. Video monitoring for flashes initially took place about 25 years ago (e.g., [6]), and they were first observed in the 1999 Leonids activity [7–9]. Lately, observations for flash detection have been conducted systematically [10–12].

A high-velocity impact with the lunar surface generates a hot vapor cloud that radiates briefly in the optical spectrum, as well as high-temperature incandescent ejecta (e.g., [13]). The radiation from impact-generated plasma-gas clouds was proposed as a source of the flashes by [14], while some laboratory experiments have found that ejecta may be a more plausible source for the bulk of the light flash signal [15,16]. On the other hand, the authors of [17] argue that the luminous events correspond to radiation emitted by both, i.e., a cloud composed of gas and small ejected melt droplets, as the duration of these transient events is typically longer than predictions based on expanding plasma-gas clouds. They also state that emission from ejecta above the surface would cover an area that must be larger than that of the resulting crater.

The light from the impact is detectable against the darker background of the lunar night side. The night side of the moon provides an immense natural screen for meteoroid detection. The counting of these flashes is useful in estimating the flux of incoming bodies to the Earth and the Moon [18].

1.1. Scientific Relevance of Impact Observations

The identification and analysis of flashes produced by the impact of meteoroids on the lunar surface are one of the techniques suitable for the study of the flux of interplanetary matter impacting the Earth [19]. Harmoniously, ref. [20] stress that the observation of LIFs has provided valuable information on the flux of meteoroids in a size range difficult to measure with conventional meteor video techniques due to the low flux at gram to kilogram sizes and a relatively small collecting area of the atmosphere over a camera site. In fact, it is worth pointing out that some works have been successful in constructing a global size–frequency distribution of meteoroids relying purely on LIF datasets [3,10].

The larger collecting area of the lunar surface provides better number statistics as the area covered by one single detection instrument (typically ~1 million km²) is much

larger than the atmospheric volume monitored by meteor detectors employed by fireball networks [19,20].

Lunar impacts also provide novel insights into high-velocity impact phenomena, since lunar impact velocities by far exceed those achievable by laboratory experiments [13]. In contrast to the relatively “slow” man-made collisions, meteoroid collisions with the Moon are capable of generating far greater energy release than spacecraft impacts; therefore, meteoroid impacts can serve as a probe for lunar water or other constituents just beneath the lunar surface [21].

The observation of lunar-meteoroid impact flashes is also motivated in the context of projects for future lunar seismological networks [22,23], the exploration of the lunar atmosphere (e.g., LADEE—lunar atmosphere and dust environment explorer), the search for new impact structures on the lunar surface (e.g., LROC—Lunar Reconnaissance Orbiter Camera), and the measurement of the largest meteoroids within the principal annual meteoroid streams [23].

Regarding the seismological implications, meteoroid impacts are reported to have caused about one-fifth of the lunar seismic events recorded by the Apollo passive seismic experiment between 1969 and 1977 [24,25].

As asserted by [22], the detection of meteor impacts on the Moon from Earth observations allows us to obtain the space/time location of seismic sources. Most of these impacts cannot be located by a lunar seismic network with fewer than three seismic stations. The Earth-based detection of impacts allows us to improve the determination of upper mantle and crustal structure by adding more data at short epicentral distances. The authors add that such meteor impact detections may be necessary to investigate the 3D structure of the lunar crust.

For the authors of [18], further research into impact frequency across the lunar surface also has the benefit of shedding light on potential lunar living areas, while seasonal and shower impact variability could be further analyzed to determine prime times of impact probability. The authors also refer to the use of high-resolution Lunar Reconnaissance Orbiter (LRO) imagery to attempt to find new craters created by observed impacts as particularly interesting. Recently, software has been developed to automatically search for impact craters associated with LIF in LRO data [26]. Considering that, in atmosphere-less bodies such as the Moon, the impactor is allowed to reach the lunar surface without breaking [3], the relationship between the observed flash and crater size could greatly advance the understanding of energy partitioning at impact events [3,18]. As a consequence of an impact on the lunar surface, the kinetic energy is partitioned into the excavation of craters, the production of plumes associated with the flash of light, and the generation of seismic waves that propagate through the lunar interior [1].

Some authors also refer to the serious motivation in regards to a better knowledge of potential hazards to the Earth. In that regard, the authors of [19] claim that Earth impact hazard estimations were not well constrained, as they found a meteoroid flux that is one order of magnitude above the estimates by previous studies, alerting for an increased impact hazard. They conclude by stating that “a systematic monitoring of moon impact flashes but also of fireballs in the Earth’s atmosphere would provide a more reliable impact frequency, especially if the luminous efficiency is well calibrated”.

1.2. Observation Campaigns and Amateur Collaboration

In view of the limitations inherent to the observation of impacts on the Moon, global observation campaigns should be organized in such a way that any detected event is reported by several observers [17]. It is also important to distribute the campaign efforts more evenly over several meteor shower periods [2].

The development of an international project (ILIAD—international lunar impacts astronomical detection) has been proposed by [18] with the objective of fostering LIF monitoring programs in several stations around the globe, arguing that permanent LIF observation programs may be run in different parts of the globe using mid-sized telescopes.

Consonantly, [17] states that the time during which the Moon is monitored must be increased, and stations outside of Europe, Japan, and the United States are required. They comment that such an effort towards the achievement of a dedicated global network would benefit the scientific community, provided that such data are made publicly available. If the number of stations is two or more in each region (same longitude), it would even be possible to increase the number of faint flash detections by using long focal length telescopes (smaller field of view but higher detection limit).

Indeed, the evolution in this field over the past two decades is worthy of great notice and that is certainly owed to the exponentially increasing quantity (and quality) of reported observations, which, in turn, has been enabled not only by technological advancements but, mostly, by the collaboration between amateur and professional communities.

The amateur contribution has been regarded as desirable for a long time, as highlighted in a relatively early work [21], in which the authors assert that collaborations between professional and amateur astronomers had already proven quite useful and mutually beneficial, especially with an increasing number of amateurs outfitted with equipment traditionally reserved for professional use, such as CCD cameras, low-resolution spectrographs, photoelectric photometers, and filters. Besides, various astronomical organizations have stepped up to encourage such collaboration, making data collected by the amateur easily accessible to the professional to assist the latter in his or her research. Organizations such as the Association of Lunar and Planetary Observers (ALPO), the International Astronomical Union (IAU), the International Occultation Timing Association (IOTA), the American Association of Variable Star Observers (AAVSO), the International Meteor Organization (IMO), and the American Astronomical Society (AAS) have been actively promoting such collaborations. The authors of [21] conclude that observations of lunar impacts provide an excellent avenue for professional–amateur collaborations, as smaller observatories and amateurs can make a serious contribution in this area by determining not only the frequency of occurrence but also the luminous energy output and spectra of these events.

As properly detailed ahead (Section 2.1), the Brazilian Meteor Observation Network (BRAMON) has become one more organization of broad reach to promote, organize, and collect observations of LIF activity, with the success of its inaugural campaign being the cause of the present study.

1.3. The Geminids Properties

The characteristics of the Geminids are summarized in [13], including their bulk density, $2.9 \times 10^3 \text{ kg m}^{-3}$, which is the highest among the meteoroids associated with major showers and the sporadic background [27], and their tensile strength, $\sim 10^5 \text{ Pa}$, which suggests that Geminids would not be fluffy aggregates, as expected for cometary materials [13]. In fact, the Geminids are found to have the lowest porosity among the main streams and the sporadic meteoroids [27]. Spectral observations of Geminids meteors show a depletion of sodium, probably due to solar heating during their perihelion [28,29]. The orbital similarity between Geminids and the asteroid 3200 Phaethon indicates that the meteoroids result from debris shed from that asteroid (reviewed in [30]), which has a perihelion distance of only 0.14 AU and is classified as one of the active asteroids [31]. The author of [32] proposed a method to calculate a meteoroid stream mass and, by applying it to the Geminid stream, found a mass of about 10^{16} – 10^{18} g with some preference for the lower mass. The author claimed that this was consistent with radar and visual observations.

2. Materials and Methods

The procedure for the optical detection of LIFs consists of searching transient luminous events using images of the non-illuminated fraction of the lunar disc. It is now well-established that detections are accessible to modest size telescopes (about 8–20 in.) observing in visible wavelengths [17].

As impact flashes can only be detected during the lunar night, [23] suggest that 10 nights of observations per lunar month must be dedicated to impact flash monitoring—5 during the waxing crescent and 5 during the waning crescent—whereas [19] asserts that the technique can be employed when the sunlit portion of the lunar disc varies between, approximately, 5 and 60 percent, i.e., during the first and last quarters.

2.1. Observing Campaign by BRAMON

From late November to early December 2017, members of the Brazilian Meteor Observation Network (BRAMON) conceived an observing campaign for LIFs after realizing that the combination of the Moon's altitude and disc illumination near the peak of the Geminid meteoroid stream would be of very favorable circumstances for observers located in Brazil. The Geminid meteor shower, among those that possess a more regular Zenith Hourly Rate (ZHR), is definitely one of the most expressive annual showers. Once the window of opportunity was identified (pre-dawn of 14 December 2017), BRAMON initiated the organization and communication of the campaign among members and other Brazilian amateur astronomers. The expected geometry of the impact flux from the Geminid stream, as the Moon crossed the densest part of it on the occasion, is shown in Figure 1.

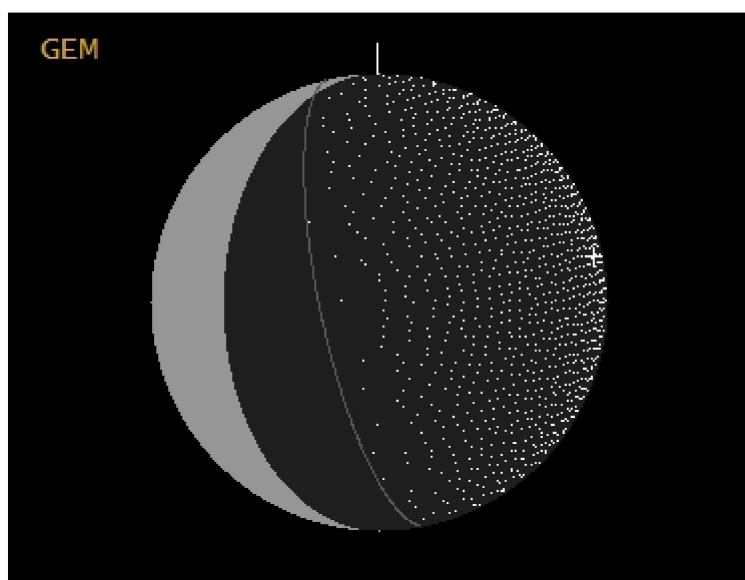


Figure 1. Impact geometry on the Moon from meteoroids of the Geminid stream, plotted by the LunarScan software for 14 December 2017.

Predictions from the LunarScan software also indicated that the stream would peak at 01:16:22 UT, with a ZHR (as seen from Earth) of 120 meteors, the Moon would rise 3.1 h before the sun, and 63% of impacts would happen on the unilluminated near side.

Observers were instructed on how to operate free recording software and which common area on the lunar disc should be monitored (nearly the whole unilluminated area, if whatsoever possible, but avoiding the terminator in order to prevent the saturation of the camera resulting from an excess of light from the illuminated part of the Moon, as noted in, e.g., [23,33]).

2.2. Observing Teams, Respective Sites, and Period of Observation

Two participant teams were successful in properly getting their equipment to monitor the Moon during the period of maximum Geminid flux in search of possible impact activity. Both were located in the northeastern coastal region of Brazil, as specified below:

- David Duarte and Romualdo Caldas, in the city of Maceió, in the state of Alagoas, at the geographical coordinates of 9°37'14"S and 35°43'12"W.

- Marcelo Zurita, in the municipality of Araruna, in the state of Paraíba, at the geographical coordinates of $6^{\circ}27'8''\text{S}$ and $35^{\circ}40'24''\text{W}$.

They agreed to start recording about one hour before daybreak, as soon as they judged the Moon was high enough above the horizon to prevent atmosphere distortion from excessive air mass, which could possibly compromise the experiment.

2.3. Observation Circumstances (Orbital, Atmospheric, and Local)

The monitoring took place during the waning crescent phase, under a Moon age of about 25.8 days, with less than 14% of disc illumination to Earth-based observers and low glare from the sunlit region. The equatorial coordinates of the Moon were 14 h 26 min 57 s in right ascension and $-9^{\circ}43'33''$ in declination at the time of Flash 1, according to the Virtual Moon Atlas (VMA) software. It should be noted that, at a distance of nearly 3.99×10^5 km, the Moon was much closer to the apogee than to the perigee.

2.3.1. Maceió

The orbital conditions—coupled with good atmospheric seeing (in spite of the low altitude over the horizon), good weather in medium, and high levels of the atmosphere (overall, good atmospheric transparency)—provided us with an exceptional resolution for live frames, which, in turn, enabled us to achieve a crisp focus, to the point of discerning major and even some minor features in the earthshine-lit lunar topography.

Terrestrial obstruction (a tree) prevented the start of the recording until the Moon reached about 15° in altitude. After the clearance of the obstruction and the passing of a huge cumuliform cloud, the view was totally unimpeded at about 06:40 UTC. We recorded for approximately 60 min until the atmosphere was lit enough to preclude any attempt to properly discern the unilluminated area of the Moon from the sky background.

2.3.2. Araruna

The Associação Paraibana de Astronomia (APA) had planned an expedition to observe the peak of the Geminid Meteor Shower from Araruna, a municipality of dark sky located in the semiarid subregion of the Northeast Region of Brazil. The lunar monitoring session would take place on that occasion. However, cloudy weather prevailed during most of that night, which hindered an accurate choice of the most suitable location to place the equipment in advance. Though the skies cleared in the last part of the night, when the Moon rose above the horizon, the team realized that a tree was causing obstruction, which resulted in the need to move the equipment, and polar alignment of the equatorial mount had to be performed again.

The recordings started at 06:03 UTC, with the Moon at an altitude of about 11° , and would continue until 07:26 UTC, with a few interruptions caused by clouds and another, between 07:14:04 and 07:16:34 UTC, owing to a lack of storage in the computer. A total of 63 min were recorded in Araruna.

2.4. Instrumentation

2.4.1. Maceió

The monitoring system at this site included a 200-mm Schmidt-Cassegrain Telescope (MEADE LX90-SC 8-inch) working with no optical accessory capable of amplifying (i.e., Barlow lens) nor reducing (focal reducer) the native focal length of the telescope. Therefore, it worked at $f/10$, resulting in a 2000-mm focal length.

The telescope mount was the computerized altazimuth Celestron NexStar 8SE, whose go-to alignment options include a “Solar System Alignment”, which demands only one point (a solar system object) in order to consider the telescope properly aligned. The Moon itself was used for that purpose, automatically resulting in a lunar tracking rate. Still, we had to recenter the object manually several times (a procedure also reported by [34]).

The images were recorded by using a ZWO ASI1600MM-Cool camera, which is monochrome and cooled, bearing a $4/3''$ CMOS sensor, measuring 21.9 mm in diagonal.

Mainly marketed towards deep-sky imaging, this camera is highly sensitive. Its native resolution is 16 Mega Pixels (4656×3520), with a pixel size of $3.8 \mu\text{m}$. This camera is theoretically capable of achieving 23 frames per second (FPS) at full resolution via a USB 3.0 interface. However, we had to use a USB 2.0 interface on this occasion. That, coupled with the relatively high exposure time necessary for the unilluminated part of the lunar disc, resulted in a speed of a little under 5 FPS (precisely, 4.46 FPS). We took advantage of the camera's built-in cooling feature, which helped with noise reduction and with the elimination of hot pixels.

The quantum efficiency (QE) of the camera sensor is provided by the manufacturer. The spectral response is expressed as $\text{QE} \cdot (e/h/c) \cdot \lambda$ where e , h , and c denote the electron's charge, the Planck constant, and the light speed, respectively. The relative spectral response of the camera employed in Maceió is calculated from the QE (see Supplementary Materials Figure S1). It is noteworthy that the curve is very similar to the spectral response of the camera used by [20], which is also burdened by a low response at the peak of a 2800 K LIF (the average peak of the spectral energy distribution of an LIF, as modeled by [35] and computed from several observations by [3]).

The software used to control the camera and record the video output to the hard drive was the SharpCap freeware. As an attempt to increase the capture speed, we used the region-of-interest (ROI) functionality, cropping the sensor area to 2640×2640 , and we also applied 2×2 binning. Thus, the effective resolution of our recordings was 1320×1320 , at $0.78''$ arcsec/pixel, capturing at 8-bit. It should be noted that, even with the cropping and the long focal length of 2 m, the attained FOV was $17'14'' \times 17'14''$, more than enough to encompass nearly all of the earthshine-lit region of the Moon, thanks to the very large sensor of the camera (see Supplementary Materials Figure S2, for the FOV of the Maceió setup). Timestamping was a functionality available within the capture software, which obtains the time from the computer clock, which, in turn, was kept synchronized by a software called Dimension 4. Both teams independently resorted to this means to achieve time correction in each of their computers.

It is worth mentioning that a 200-mm focal length is commented on in [17] as a good option to increase the resolution and, therefore, the flash/earthshine ratio, allowing for the detection of smaller sub-pixel flashes, and a large sensor chip may be used to maintain a large field of view. That was precisely what the combination of the 200-mm f/10 telescope with the camera described above delivered here.

2.4.2. Araruna

A 130-mm Newtonian telescope was used in Araruna, working in prime focus, at its native focal length (650 mm), and the sensor was a typical closed-circuit television (CCTV) camera, namely, a Samsung SCB-2000. A motorized EQ3-2 equatorial mount allowed for the tracking of the relative lunar motion, with manual corrections applied by the arrow keys of its hand controller whenever needed.

The Samsung SCB-2000 has a $1/3''$ Super HAD CCD color sensor, providing a native resolution of 768×494 pixels, outputting an NTSC interlaced analog signal.

The effective FOV of the setup was $26'06'' \times 17'24''$. It should be noted that, although the camera is originally provided with an infrared cut-off filter, this had been removed.

Conversion from analog to digital signal was achieved by the EasyCap USB capture card, which delivered the digital video in RAW format, YUY2 color space, at a frame rate of 29.997 FPS and a resolution of 720×480 pixels. The greyscale information extracted from the format was used for the photometric analyses described later.

As in Maceió, the SharpCap freeware was used to provide the computer interface with the camera and, thus, enable the recordings, which were made at 30 fps and 720×480 .

2.5. Verification for Flash Candidates

Impact flashes are very short in duration (most of them are contained in just one or a few video frames). Therefore, their identification by hand is not practical and computer

software is required to automatically identify impact candidates [18]. In this regard, it is worth mentioning the novel approaches recently proposed by [3].

However, analogous to several previous studies [10,18,23,36], we used the LunarScan software (developed by Peter Gural) on the recorded videos to perform automated detections of transient events in the field of view. LunarScan determines impact candidates by searching for clusters of pixels that exceed the set threshold above the lunar background; the candidates are displayed for user confirmation upon completion of the analysis [18]. The software imposes two limits on the video files: the resolution cannot exceed 720×480 , and the file size must be smaller than 1 GB. The resolution limit did not pose any restriction to the original files from Araruna. However, the videos acquired by the Maceió team exceeded both of those limits by far. Therefore, we resorted to the VirtualDub software to crop the videos into six sections smaller than or equal to 720×480 —which is the reason for the appearance of a much smaller FOV, e.g., in Figures 2 and 3, than in the original frames (see Supplementary Materials Figure S2, for the whole FOV)—and then each section was trimmed to clips that would not surpass 1 GB.



Figure 2. LunarScan windows displaying Flash 1 from the Maceió recording.

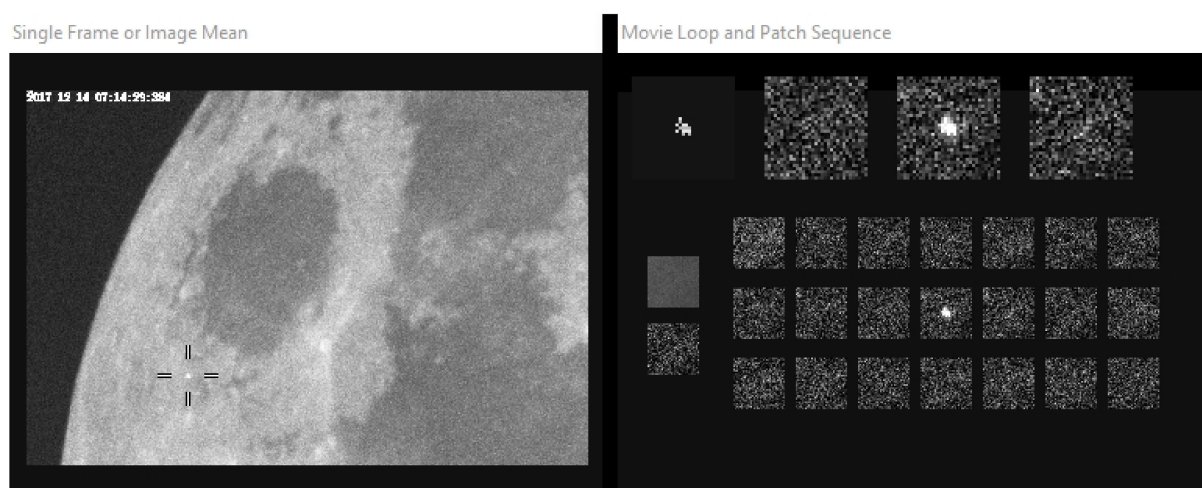


Figure 3. LunarScan windows displaying Flash 2 (recorded only from Maceió).

In LunarScan, the default settings were applied. The first step was setting the masking and processing areas, as well as indicating the lunar surface parameter. This is necessary to purposely ignore some regions during the process, so as to prevent a large number of false detections [37].

The next step was the execution of the automatic scanning function. Nonetheless, even with the masks applied and the processing area properly indicated, a variety of other physical phenomena can cause false positives, including cosmic rays, instrument noise, and satellites [18]. Hence, the automatically detected transient events must be manually examined in order to shortlist the detections that present the typical characteristics of impact flashes in terms of intensity, spatial extension, and duration [23]. This was carried out by the consecutive LunarScan step, “4 = Confirmation of Impacts”, by which all the detected transient events are presented to the software user, who can either confirm or ignore/eliminate each one. If any flash is selected as confirmed by the user, two TIFF files are generated in inverted colors: one is a sequence of 7 frames centered around the peak of the brightness of the flash, as seen in Figure 4, and the other is the whole specific frame that contained the peak in luminosity (see Supplementary Materials Figures S3–S5).

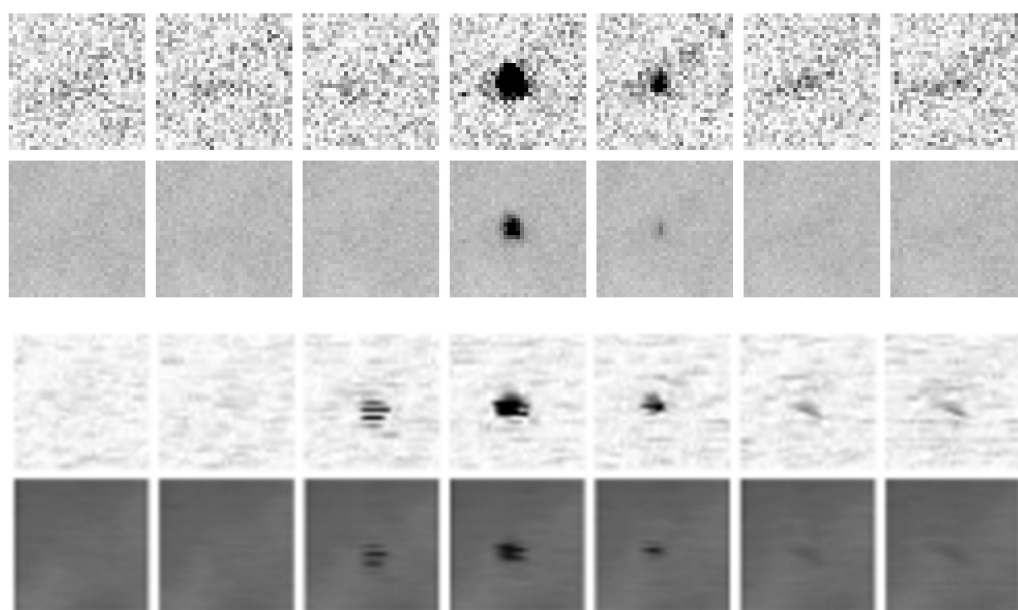


Figure 4. TIFF files of a seven-frame sequence generated by LunarScan for Flash 1, from the recordings at Maceió at 4.46 FPS (**top**), and Araruna at 30 FPS (**bottom**), inverted colors.

3. Results and Discussion

3.1. Identified Flashes

After discarding all evident false positives (with the more frequent being the displacement of features of highest albedo in the Lunar surface due to imperfect tracking), we were left with two very promising impact flash candidates (Figures 2 and 3).

The first occurred at 07:13:46.7 UT and was recorded by both teams. The perceived flash brightness (above the lunar background) lasted for two video frames for the Maceió observation setup (Figures 2 and 4), at a frame rate of 4.46 FPS, and for ten video frames for the Araruna setup (Figure 5), which was recording at 30 FPS. Considering the number of frames exhibiting the flash and the timelapse (exposure time) of the frames of the observation setup at Araruna—0.033 s—Flash 1 reached a total duration of 0.33 s. The frame duration of the Maceió setup is 0.224 s, therefore, as the duration of Flash 1 is shorter than the sum of the two detection frames at Maceió, i.e., 0.448 s, the flash would begin at some point during the first exposure and end in the early portion of the second exposure.

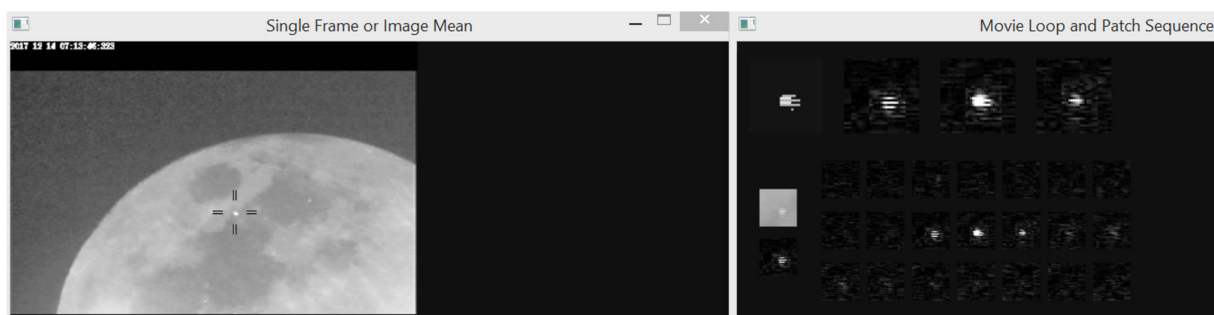


Figure 5. LunarScan windows displaying Flash 1 from the Araruna recording.

The second flash happened at 07:14:29.4 UT, and, although only 43 s after the first one, it was recorded solely by the Maceió team, as the hard drive used at Araruna filled up and stopped recording almost immediately after the detection of Flash 1. This second event was much shorter in duration than the first one, being perceived from Maceió in an unequivocal way by a single frame only (Figure 3). See also the Supplementary Materials Figure S6, for the seven-frame sequence of Flash 2 retrieved by LunarScan from the Maceió recordings.

At about 04:14 in local time, both flashes (separated by merely 43 s) happened when the sun was at an altitude of -10.5° , in early Nautical dawn, but the inherent twilight conditions were still negligible. The Moon was at an altitude of about 27° from both sites, as they share practically the same longitude. It is worth clarifying that the other teams in Brazil who took part in the BRAMON observation campaign experienced bad weather. We also checked with other organizations, such as ALPO and NASA's Marshall Space Flight Center, in order to know of any possible international detection of these events, but there were none. Since the eastern coastal region of the Brazilian Northeast is geographically a protrusion of South America towards the Atlantic, this could be expected, as few other inhabited regions would have the Moon in the narrow altitude interval where it would be high enough in terms of air mass and clearance of obstructions yet still low enough to not be affected by twilight.

3.2. Confirmation of Lunar Activity Nature

The affirmation of the lunar impact nature regarding Flash 1 stands on a solid foundation, especially because there is a second simultaneous and independent observation of the flash at the same selenographic coordinates. The two independent observations discard false detections produced by other phenomena, such as satellite glint, cosmic rays, and electric noise (e.g., [21]). To eliminate the possibility of satellite glints, the two observations must be made from locations far from each other.

A minimum separation of 50 km between the sites is recommended by [21], while another study affirms that a distance of 10 km suffices [36]. However, what is important is not the distance between the sites but the parallax from the two sites. Consider the following situation: a lunar flash is observed from two observatories when the moon is close to the horizon and the moon and the two observatories are almost in a straight line. In this case, both the parallax of the moon and the parallax of a satellite on the straight line are almost zero. It would be difficult to discard the possibility of the satellite glint even though the observatories are separated 50 km from each other. On the other hand, if the moon is close to the zenith, the parallaxes of the moon and a satellite would differ enough to be detected even though the observatories are separated only 10 km from each other.

Although the separation of 353 km between Maceio and Araruna seems to be enough to discard the possibility of a satellite glint, it is necessary to check whether the parallax rules out a sun glint flash of low earth orbit or geosynchronous satellites or space debris. We have therefore performed parallax calculations. The parallax from the two observatories, Maceio and Araruna, was obtained for a hypothetical satellite at an altitude of 40,000 km above the observatories in the lunar direction from their perspective. The result is 1800 arcsec (which

is about the angular diameter of the Moon). As the Moon is located ten times farther, and its parallax is 180 arcsec, the difference between the two parallaxes, 1620 arcsec, would have been easily perceived in our observations.

It should be noted that, in addition to being simultaneously observed from two sites and with a separation between them that far exceeds the threshold for eliminating any possible parallax effect from a satellite glint, Flash 1 also presented every other characteristic of a lunar impact event, including multi-frame detection, an asymmetric light curve, a star-like appearance, and no relative movement from frame to frame (e.g., [21]).

As for Flash 2, it was observed only from Maceió because of the pause in the recording from Araruna. However, considering that it has a star-like appearance, not resembling at all the typical cosmic ray shapes nor electric noise, this favors the possibility of a lunar impact nature for the second flash.

3.3. Positioning on the Lunar Surface

For performing the estimation of the impact coordinates of both flashes, we used the images acquired in Maceió (the 200 mm telescope and the ASI1600MM camera), since they had a superior spatial resolution.

The high-precision positioning of LIFs has, naturally, the importance of offering the possibility of comparing new and prior images of the Moon to look for impact structures associated with the flash [23].

In addition to that, [17] emphasizes the relevance for future missions devoted to the seismological exploration of the Moon. They assert that poor knowledge of impactor location precludes any correction of signal amplitudes for propagation effects. The distance between the seismic epicenter (impact position) and a seismic station must be known accurately to derive the seismic velocity in the lunar interior.

As stated in [23], owing to the fact that LIFs are monitored on the non-illuminated fraction of the lunar disc, the frames in which the flashes are detected are often nearly featureless, with early works having resorted to astrometry techniques to model the lunar configuration at the time of observation. Such was the case of [2], in which the coordinates of the center of the lunar disk were determined from the curvature of the night-side lunar rim and field stars. Then, the selenographic coordinates of the flash were retrieved from the angular distance and position angle (both relative to the lunar disk center) of the flash, taking lunar libration into account.

More recent methods for deriving the position of LIFs have relied on specific tools of self-developed software, e.g., MIDAS [33] and NELIOTA-DET [12]. The first performs a calibration that takes into account the known position of at least three different features on the lunar surface and then automatically provides the LIF (x,y) coordinates and the corresponding values of latitude and longitude. The latter is semi-automatic and based on a cross-match with images from the detailed lunar map provided by the VMA software after some processing steps, which are described in [12]. In fact, a number of other studies have used VMA images as a reference for positioning, e.g., [13,36]. Another interesting and much more complex automated approach has been recently proposed [3].

Here, we partially follow the technique described in [23], which is claimed by the authors of that work to be suitable when observations are performed soon after or before the new moon, with the earthshine bright enough to make it possible to recognize features in the Lunar terrain. As previously stated (Section 2.3), that was precisely the case here. The orbital and atmospheric circumstances could not get much better than what we experienced. Moreover, the instrumentation of the team at Maceió provided crisp spatial resolution, as noted in Section 2.4.1. A very good optical resolution and a high signal-to-noise ratio (SNR)—which, in turn, delivered a considerably bright earthshine-lit lunar region—endowed us with enough visual information to determine the location of the first impact. The method proposed by [23] consists of stacking a certain number of frames in order to increase the SNR and produce an optimal image of the non-illuminated fraction of the Moon. In our case, we selected 150 frames starting from a few frames after

the last frame in which the flash was detected. Then, the AutoStakkert! software was used to stack the best 100 frames among that total according to its inherent analysis algorithm, which selects frames based on their definition, with a technique called “lucky imaging”. A comparison between a raw frame and the stacked image is exhibited in Figure 6. The SNR and the definition are indeed highly improved through the stacking technique. The first frame in which Flash 1 was detected was then superimposed on the stacked image and carefully adjusted to match the surface features between the two images. After that, the flash area was selected to generate a mask that showed only that particular area of the first frame of Flash 1 on the stacked image. This resulted in Figure 7, which exhibits the flash area on an image that is much richer in recognizable surface features than the original.

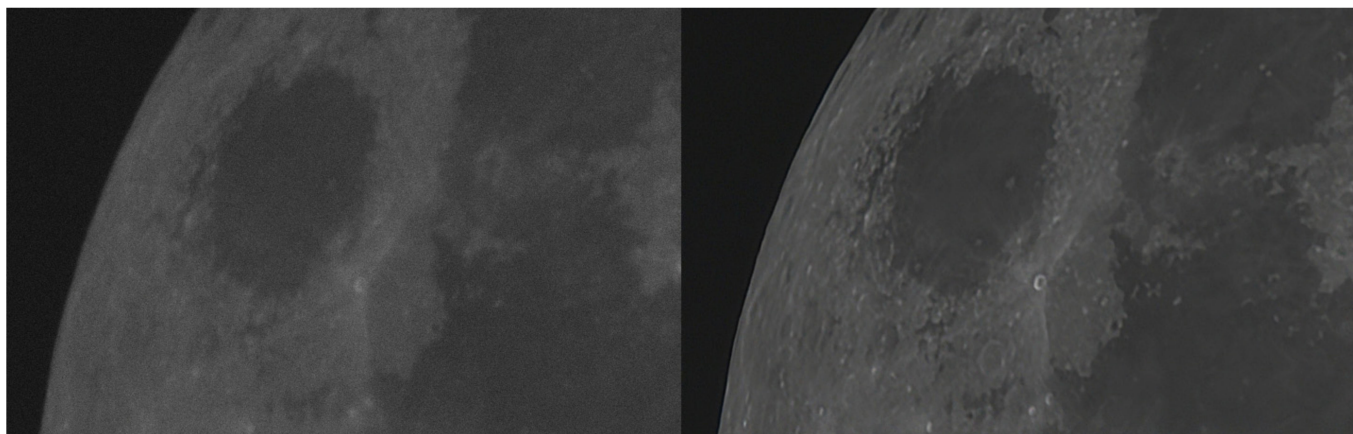


Figure 6. A single raw frame near the detection frame of Flash 1 (**left**). Stack of 100 video frames among the 150 that followed the last frame where Flash 1 was detected (**right**). Data from Maceió.



Figure 7. Flash 1 represented on the stacked image.

From that, it was possible to reach the next step, which consisted of accurately superimposing the flash area on an image that was georeferenced (or, perhaps more accurately,

“selenographically” referenced). Such an image was acquired from the VMA software, in which it is possible to set the date and time (which is important to account for libration, for instance, as also noted by [12,13,36]), and obtain a gridded image for that moment. Figure 7 was then cropped, rescaled, and rotated in order to carefully match the underlying reference image from the VMA software.

Then, once again, a mask resource was used to isolate the flash area from the overlying image, resulting in an image of the VMA with the flash area represented on it (Figure 8). At this point, the selenographic coordinates of the flash could be already obtained, but, as the flash is spread over a relatively large area, the accuracy would not be as satisfactory as what the quality of our data could provide. Therefore, we resorted to a combination of two functionalities of the GIMP software—namely, the Gaussian Blur filter and the Threshold tool—to determine the barycentre of the flash by finding the very peak of the flash intensity. In this case, the Gaussian Blur filter was used as a smoothing tool on the flash area in multiple iterations, up to the point where the Threshold tool could output a single pixel, representing the peak of brightness as a point instead of a plateau.

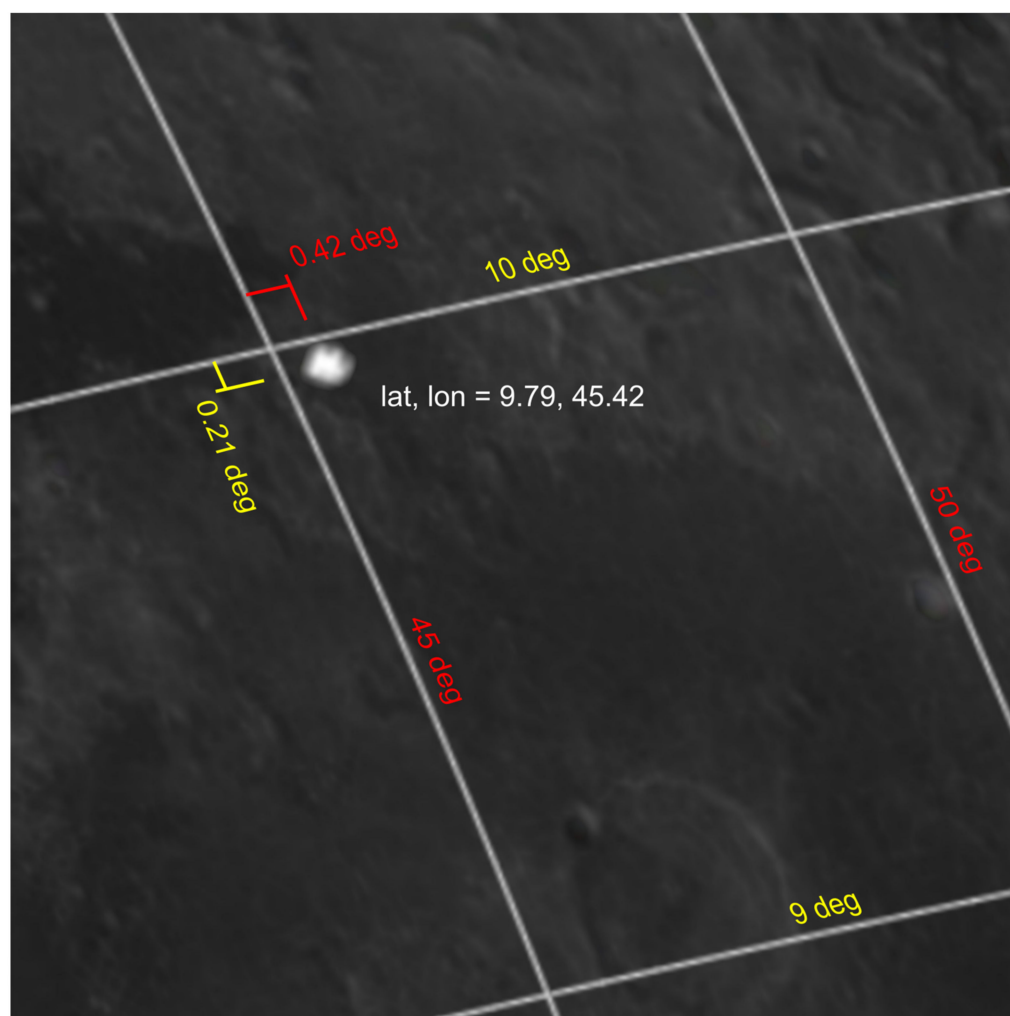


Figure 8. The location of the barycentre of Flash 1 in selenographic coordinates.

The selenographic coordinates of that pixel were calculated from the distance between the nearest grid lines and the pixel location. Those measurements, as well as the resulting values of latitude and longitude, are exhibited in Figure 8.

The positive values for both coordinates mean that the impact happened in the north-eastern quadrant of the nearside of the Moon. Each pixel on that image has the following dimensions in latitude \times longitude degrees: 0.0551×0.0725 . The pixel is elongated in

the east–west direction because it happened much nearer to the lunar equator than to the central meridian. Given the quality of the data and the methods employed, the adoption of the uncertainty of a one-pixel radius is more than reasonable. Therefore, the coordinates of Flash 1 are $9.79^\circ (\pm 0.06^\circ)$ N and $45.42 (\pm 0.07^\circ)$ E.

The procedure for obtaining the selenographic coordinates of Flash 2 was in every way analogous to the one described above for Flash 1. Figure 9 shows the last steps of the procedure. The coordinates of Flash 2 are $26.99^\circ (\pm 0.1^\circ)$ N and $57.93^\circ (\pm 0.1^\circ)$ E, on the southeastern edge of Cleomedes.

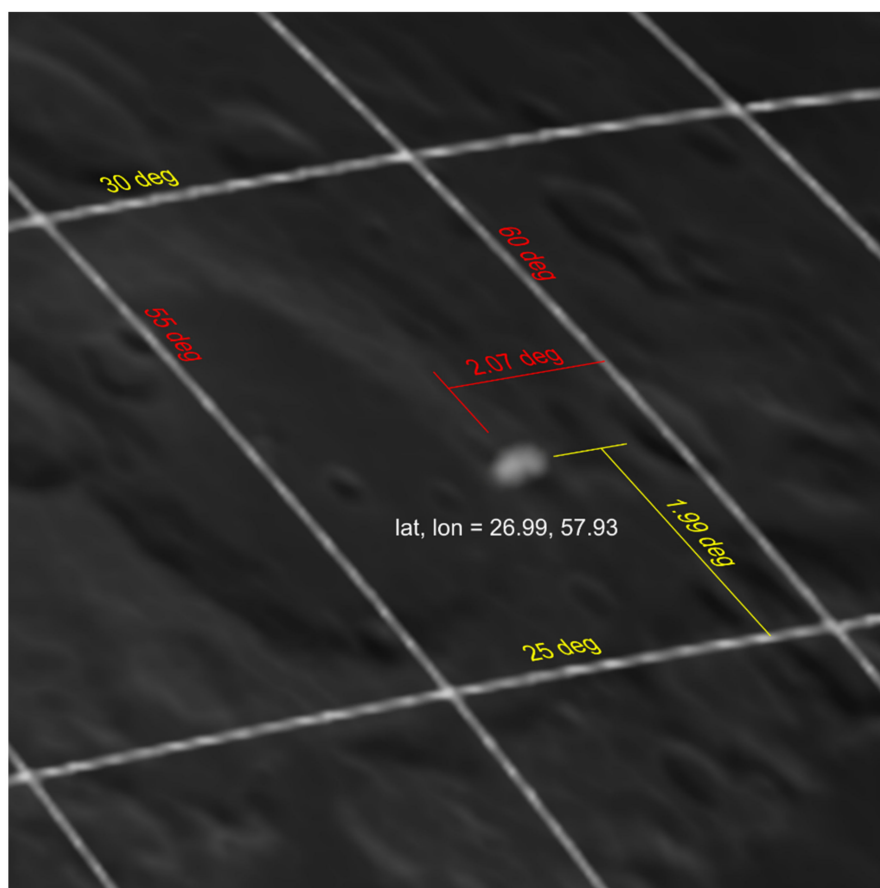


Figure 9. The location of the barycentre of Flash 2 in selenographic coordinates.

3.4. Photometry

3.4.1. Gamma Value Uniformization

The pixel value (e.g., 0–255) of an image, that is, the output of any video camera, is not necessarily proportional to the real brightness of an object. The relationship between the output and the real brightness is characterized by the so-called gamma value. It is unitary when the output is equal to the real brightness. However, it is typically 0.45 in many commercial CCTV cameras. The gamma value that was set for the camera in Maceió is known to be the manufacturer’s standard (gamma = 1.0). However, the capture software imposes limits on the settings of the camera used in Araruna, so that the gamma value set during the recording in that location had to be determined by other means.

Considering an area of 63×63 pixels in each of the regions—Mare Crisium, the Newcomb crater region, and the sky background, all in the same frame of the AVI video file recorded in Maceió—the count ratio of Newcomb to Crisium, after the correction of the sky, was 1.8. The same procedure for the video recorded in Araruna shows a ratio of 1.6 when no gamma correction is applied.

Assuming a gamma value of 0.45 and making the following correction, the ratio is found to be 1.8, which agrees with the Maceio ratio, where q is the count (0–255) for each pixel in a video frame, and q' is the corrected count:

$$q' = \left(\frac{q}{255} \right)^{1/0.45} \cdot 255 \quad (1)$$

With the correction applied, the time-integrated brightness—that is, the luminous energy—of Flash 1, calculated for both Maceio and Araruna, is nearly identical. Without the correction, the peak brightness decreases to 66% and disagrees with the result for Maceio. Therefore, the gamma value of the camera employed in the Araruna recordings must have been 0.45.

3.4.2. Count Ratio between Mare Crisium and TYC5564-94-1

The ratio between the count of the comparison star, TYC5564-94-1, and the count per square arcsec at the central region of Mare Crisium, r_{star} , was obtained after the subtraction of the background.

3.4.3. Count Ratio between the Flashes and Mare Crisium

The pixel values in boxes of 19×19 px and 7×8 px comprising the flash areas in the videos recorded in, respectively, Araruna and Maceio, were counted to obtain a flash count. The sum of the same area in video frames before and after the flash was used as a background. After background correction for the flash, the ratio between the flash count and the count per square arcsec at the central region of Mare Crisium, r_{flash} , was obtained. The brightness ratio between the flash and the star can then be derived as r_{flash}/r_{star} .

3.4.4. Light Curves

Following the methods described above, the light curves are presented as a brightness ratio of the flashes to the comparison star, TYC5564-94-1 (HD128080), in the y -axis. Figure 10 shows the light curve of Flash 1 as observed from Araruna, whereas Figure 11 exhibits the light curve according to data obtained in Maceio. The light curve of Flash 2 can be seen in Figure 12.

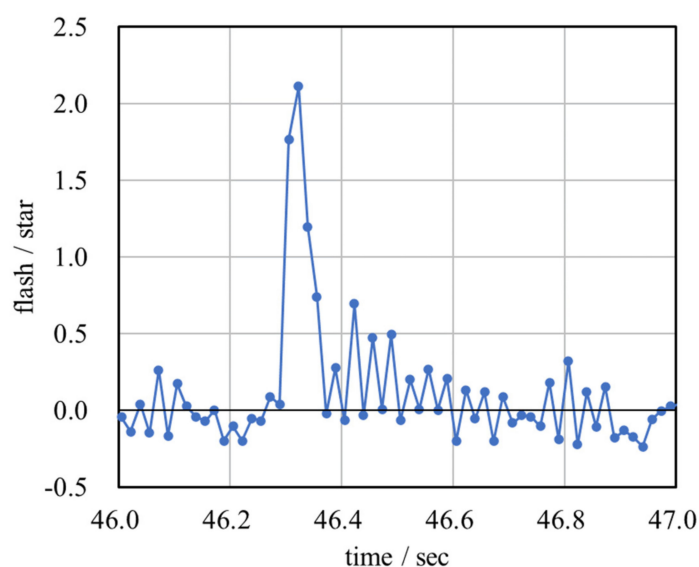


Figure 10. Light curve of Flash 1 as seen from Araruna, in brightness ratio of the flash to the comparison star.

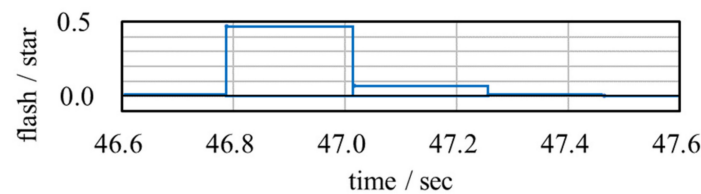


Figure 11. Light curve of Flash 1 as seen from Maceió, in brightness ratio of the flash to the comparison star.

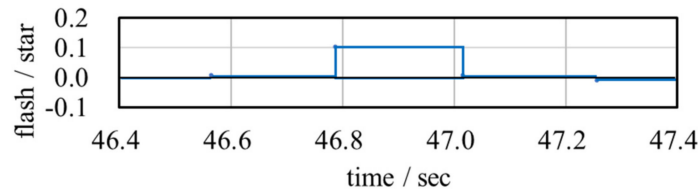


Figure 12. Light curve of Flash 2 as seen from Maceió, in brightness ratio of the flash to the comparison star.

The framing rate of the Araruna camera is 30 frames/s. Each frame consists of an odd field and an even field. The odd field is exposed for the first 1/60 s, then, the even field is exposed for the next 1/60 s. We separated each frame into these two fields, obtaining the time resolution of 1/60 s.

Flash 1 appeared darker in the observation carried out in Maceio because of the longer exposure time. This is an important result, as it shows that peak magnitudes depend on the exposure time of cameras [13]. Another important observation is that it is particularly noisy between 46.4 and 46.6 sec in Figure 10. The conversion from an analog signal to an AVI file may have caused this.

3.5. Spectral Flux of the Flashes

3.5.1. Spectral Flux of the Comparison Star

TYC5564-94-1 (HD128080) is a K4III giant star of $B = 10.13$ and $V = 8.60$, according to the SIMBAD database (<http://simbad.cfa.harvard.edu/simbad/sim-fid>, accessed on 17 March 2021). Its effective temperature is 3926 K, according to [38]. We assumed that its spectral flux was approximated as $g_{star} \cdot \pi \cdot B(3926K, \lambda)$ [W/m²/nm], where B is the Planck function, and it is multiplied by π steradian. g_{star} was determined to satisfy the following equation:

$$V_{star} - V_{A0} = -2.5 \log_{10} \frac{\int g_{star} \cdot \pi \cdot B(T_{star}, \lambda) \cdot f_V(\lambda) \cdot d\lambda}{\int g_{A0} \cdot \pi \cdot B(T_{A0}, \lambda) \cdot f_V(\lambda) \cdot d\lambda} \quad (2)$$

Here, V_{star} is the V-magnitude of the comparison star (8.60) and V_{A0} is the V-magnitude of Vega (0), while $f_V(\lambda)$ represents the response function for the V-band in the Johnson–Cousins UBVRI photometric system, as shown in [39], as the SIMBAD database shows B_T and V_T in the Tycho-2 Catalogue, which is close to the Johnson B and V.

A0V type stars such as Vega (α -Lyr) are the standard of the astronomical photometric system. Its temperature is 9600 K, and its magnitude is the same for all bands. We approximated the spectral flux of an A0V type star of $B = V = R = 0$ as $g_{A0} \cdot \pi \cdot B(9600 K, \lambda)$ [W/m²/nm]. g_{A0} was determined, so that the flux at $\lambda = 555.6$ nm is 3.56×10^{-11} W/m²/nm, as in [40].

The calculation of the integrations in the equation was done numerically by summing the cell values in spreadsheet software and multiplying it by $d\lambda$ (10 nm).

3.5.2. Spectral Flux of a Flash

The flashes are assumed to be radiating as black bodies of 2800 K [3,10,35]. The spectra of Geminids LIFs shown by [13] support this assumption. Hereinafter, for all the relevant

calculations, both flashes will be assumed to have been caused by Geminid impactors (see Section 3.8).

Therefore, the spectral flux of a flash was modeled as $g_{flash} \cdot \pi \cdot B(2800\text{ K}, \lambda)$:

$$\frac{r_{flash}}{r_{star}} = \frac{\int g_{flash} \cdot \pi \cdot B(2800\text{ K}, \lambda) \cdot f_C(\lambda) \cdot d\lambda}{\int g_{star} \cdot \pi \cdot B(3926\text{ K}, \lambda) \cdot f_C(\lambda) \cdot d\lambda} \quad (3)$$

The left-hand term is the brightness ratio between the flash and the star, plotted in Figures 10–12.

f_C is the response function that combines the camera's spectral response curve and the atmospheric transmittance found in [41].

3.5.3. Magnitude Calculation

The R-magnitude of each flash was calculated according to the following formula, where f_R is the response function of the R-band in the Johnson-Cousins UBVRI photometric system [39].

$$R - 0 = -2.5 \log_{10} \frac{\int g_{flash} \cdot \pi \cdot B(2800\text{ K}, \lambda) \cdot f_R(\lambda) \cdot d\lambda}{\int g_{A0} \cdot \pi \cdot B(9600\text{ K}, \lambda) \cdot f_R(\lambda) \cdot d\lambda} \quad (4)$$

The V-magnitude was obtained analogously.

Resultantly, the peak magnitudes for the V and R bands of Flash 1, as measured according to Araruna's data, are 7.4 and 6.3, respectively, whereas, according to the data collected at Maceió, those same quantities present the values of 9.0 and 7.9. In regards to Flash 2, data from Maceió indicates a peak V-magnitude of 10.7 and a peak magnitude of 9.6 in the R-band. These results are summarized in Table 1.

Table 1. Summary of the results obtained from the observations.

	Flash 1 (Araruna)	Flash 1 (Maceió)	Flash 2 (Maceió)
Peak V-magnitude	7.4	(9.0)	(10.7)
Peak R-magnitude	6.3	(7.9)	(9.6)
Impact energy	8.7×10^8 J	1.1×10^9 J	2.1×10^8 J
Meteoroid mass	1.6 kg	2.0 kg	0.38 kg
Meteoroid diameter	10 cm	11 cm	6.3 cm
Impact angle	48°	48°	56°
Crater diameter	8.4 m	8.9 m	5.7 m

Note: the magnitudes in parentheses are the ones obtained by the long exposure observation.

The differences in the V- and R-magnitudes of 1.6 between Araruna and Maceio are due to the difference in the exposure time between them. The bright phase of Flash 1 lasted less than 0.1 s (Figure 10). The luminous energy of the flash is averaged out into the long exposure time at Maceio, as far as magnitude calculation is concerned. Conversely, the peak magnitudes could be lower (brighter) if the exposure time at Araruna was shorter than 1/60 s. Thus, the peak magnitudes are just a guide to the scale of luminous energy [13].

The field interval is 1/60 s, that is, one-half of the frame interval of the interlaced TV signal. Because the temporal resolution of the human eye is about 1/60 s, the magnitudes obtained at Araruna are adopted as the nominal magnitudes in this work.

3.6. Impact Energy, Meteoroid Mass, and Diameter

If we assume that the flash radiates uniformly into 3π steradians on the lunar surface, as in [42,43], and the distance between the flash and observers is r , the luminous flux on the lunar surface is derived from:

$$S(t) = 3\pi r^2 \cdot \int g_{flash} \cdot \pi \cdot B(2800\text{ K}, \lambda) \cdot f_C(\lambda) \cdot d\lambda \quad (5)$$

where f_C is the response function obtained from the camera's QE curve.

The luminous energy, with respect to the camera's response function, is obtained as follows:

$$E_{lum} = \sum S(t) \cdot \Delta t \quad (6)$$

where Δt is the exposure time of the camera. The summation is over the frames where the flash is identified.

The impact energy is calculated as follows, where η is the luminous efficiency (set to 0.2%, according to [42,43]):

$$E_{imp} = E_{lum} / \eta \quad (7)$$

The impact energy is the kinetic energy of the meteoroids.

To obtain the meteoroid mass associated with the flash, the impact velocity must be known. We adopted 33 km/s, the geocentric velocity of Geminids. The impact velocity of Geminids at the top of the terrestrial atmosphere after acceleration by Earth's gravity is 35 km/s. However, the gravity acceleration by the Moon is much weaker, incapable of significantly altering the impact velocity of the Geminid meteoroids that collide on its surface, which thus remains at 33 km/s.

From that, the following results arise for the impact energy of Flash 1, conforming to the Araruna and Maceió observations, respectively: 8.7×10^8 J and 1.1×10^9 J, which correspond to a mass of 1.6 kg, according to data from Araruna, and of 2.0 kg, according to data from Maceió. Concerning Flash 2, our calculations pointed to an impact energy of 2.1×10^8 J, and hence a mass of 0.38 kg.

The density of Geminid meteoroids is estimated to be 2.9×10^3 kg m⁻³ by [44]. Assuming a spherical shape for the meteoroids, their diameters can be easily obtained. For Flash 1, the impactor is estimated to measure 10 cm in diameter from data obtained at Araruna and 11 cm from the Maceió site, from which we also calculated a diameter of 6.3 cm for the possible impactor of Flash 2. These results are also displayed in Table 1.

3.7. Crater Diameter

For the calculation of the resulting lunar crater, we resorted to the formula proposed by [45] for lunar craters. The equation can be found in the textbook by [14]. We adopted the value of 1.6×10^3 kg m⁻³ for the lunar regolith density, as suggested by [46].

The impact angles measured from the local lunar horizons were calculated from the Geminids' radiant direction, the lunar directions, and the selenographic coordinates mentioned in Section 3.3.

Therefore, in accordance with the aforementioned data, the obtained impact angle for Flash 1 was 48 degrees, producing a crater whose diameter should measure 8.4 m according to data from Araruna, or 8.9 m according to the observations carried out in Maceió.

Regarding Flash 2, provided that this was an impact as well, it must have happened at an angle of 56 degrees, forming a crater of 5.7 m in diameter, as shown in Table 1.

3.8. On the Geminid Source of the Impactors

The observed flash happening only a couple of hours after the activity peak of the Geminids is a strong argument in favor of the assumption that the impactor belonged to that meteoroid stream.

According to the International Meteor Organization (IMO), the reported ZHR of the Geminid meteor shower in 2017 confirms that the peak occurred during the first hours of 14 December, and the ZHR at the very moment of the impact flash reported here was about 130 meteors per hour (see Supplementary Materials Figure S7).

Nonetheless, we proceed with the calculation of the probability that the observed flashes are associated with Geminids, following the equations proposed by [11,37]. We

considered only Geminids and sporadic meteoroids as possible sources for Flash 1 and Flash 2. The probability p^{GEM} is written as follows:

$$p^{GEM} = \frac{N^{GEM}}{N^{GEM} + N^{SPO}} \quad (8)$$

where the superscripts *GEM* and *SPO* denote, respectively, Geminids and sporadic meteoroids. N^{GEM} and N^{SPO} are given by:

$$N^{GEM} = v^{GEM} \cdot \gamma^{GEM} \cdot \cos \phi \cdot ZHR^{GEM} \quad (9)$$

and

$$N^{SPO} = v^{SPO} \cdot \gamma^{SPO} \cdot HR^{SPO} \quad (10)$$

where:

ZHR^{GEM} is the terrestrial ZHR of the Geminids at the time of the flash detection.

HR^{SPO} is the terrestrial hourly rate of sporadic meteors.

ϕ represents the Geminids' meteoroid incident angle at the flash location measured from the local lunar vertical.

γ is the correction for the difference of the gravitational attraction between the Moon and the Earth, and is given by:

$$\gamma^{GEM} = \left(1 + \frac{V_{Moon}^2}{V_{GEM}^2}\right) / \left(1 + \frac{V_{Earth}^2}{V_{GEM}^2}\right) \quad (11)$$

$$\gamma^{SPO} = \left(1 + \frac{V_{Moon}^2}{V_{SPO}^2}\right) / \left(1 + \frac{V_{Earth}^2}{V_{SPO}^2}\right) \quad (12)$$

where V_{Moon} and V_{Earth} are the gravitational escape velocities of the Moon and the Earth, respectively.

V_{GEM} and V_{SPO} are the geocentric velocities of Geminids and sporadic meteoroids, respectively. V_{GEM} is 33 km/s, as discussed above (Section 3.6). As for V_{SPO} , most LIF studies have shown a preference for the value of 17 km/s [12,22], whereas others have adopted the one of 24 km/s [10]. Here, the standard of 17 km/s was embraced for the probability calculations.

The masses of meteoroids that cause LIFs are much larger than those that cause terrestrial meteors. At the same time, the meteoroids' number depends on the mass. The correction for the difference in number is represented by v :

$$v^{GEM} = \left(m_{min}^{GEM} / m_0^{GEM}\right)^{1-s^{GEM}}$$

$$m_{min}^{GEM} = E_{min} / (V_{GEM}^2 / 2)$$

$$v^{SPO} = \left(m_{min}^{SPO} / m_0^{SPO}\right)^{1-s^{SPO}}$$

$$m_{min}^{SPO} = E_{min} / (V_{SPO}^2 / 2)$$

where s represents the mass index and is related to the population index, r , via the following equation:

$$s = 1 + 2.5 \cdot \log_{10}(r)$$

m_0 is the mass for the terrestrial meteor of magnitude 6.5. m_{min} is the minimum mass for a meteoroid to be detected as an LIF. E_{min} is the minimum for a meteoroid's kinetic energy to be detected as an LIF.

We used the parameters shown in Table 2 and obtained the probabilities of 89% for Flash 1 and 90% for Flash 2.

Table 2. Parameters used to calculate the probabilities of a Geminid source of the impactors.

Parameter	Value	Remarks
ZHR^{GEM}	126/h	see Figure S7
HR^{SPO}	10/h	[11,12,34,37]
V_{GEM}	33 km/s	
V_{SPO}	17 km/s	[4,12,34]
V_{Moon}	2.4 km/s	
V_{Earth}	11.2 km/s	
r^{GEM}	2.6	IMO Meteor Shower Calendar 2017
r^{SPO}	3.0	[12,34]
m_0^{GEM}	4.5×10^{-7} kg	[34]
m_0^{SPO}	9.8×10^{-6} kg	[12]
E_{min}	2.1×10^7 J	1/10 of the impact energy of Flash 2
φ	42°	for Flash 1
φ	34°	for Flash 2

We assumed E_{min} to be one-tenth of the impact energy of Flash 2. If we decrease or increase this value by an order of magnitude, the probabilities do not essentially change and stay above 85%.

4. Conclusions

The fulfillment of all the criteria found in the literature is more than enough to confirm the lunar impact nature of Flash 1, recorded by both teams, separated by about 353 km, at 07:13:46 UT on 14 December 2017. Regarding Flash 2, which happened moments later, at 07:14:29 UT, ultimate confirmation is not possible due to the lack of a second observation. However, its luminous characteristics do not resemble or indicate any of the known typical false positives. Therefore, we presented here the calculations of the impact properties considering the assumption that it was, like the first one, produced by a lunar impact.

It is worth mentioning that the two observing setups, whose significant technical discrepancies could be prematurely considered undesirable, ended up being of a satisfactorily complementary nature. Araruna (at 30 FPS) delivered a profuse number of detection frames for Flash 1, though its spatial resolution was relatively low. The recording from Maceió rendered an excellent pinpoint definition of the selenographic location of the flashes, while the temporal resolution was not ideal (slower than 5 FPS).

This was probably the first unique observation of lunar flashes simultaneously made by a pair of instrumentation setups comprising a normal framerate camera and a long-exposure camera. The results clearly show that the peak brightness magnitude depends on the cameras' exposure time. The shorter the exposure time, the brighter the flashes would appear. We must recognize the dependence of the magnitude on the exposure time. Therefore, we adopted the magnitude for the faster exposure time of Araruna (about 1/60 s), which is the average temporal resolution of the human eye, as nominal for Flash 1.

The exceptional spatial resolution and SNR provided by the instrumentation in Maceió, resulting from a relatively long focal length, large telescopic aperture, favorable weather conditions, and, most differentially from other works, the camera's low readout noise and long exposure time, enabled a positioning method for the flashes that is safely based on the lunar surface features, with a very low uncertainty of only ± 0.06 degrees in latitude and ± 0.07 degrees in longitude for Flash 1. Such a level of precision regarding the impact location will certainly aid in finding associated craters from images from the LRO spacecraft, in addition to helping lunar seismological observations in the future.

In view of the successful results accomplished by this experience, national observing campaigns of this kind will be given continuation, envisioning an ever-increasing number of observers and improvements of all sorts, in addition to seeking and fostering international cooperation.

Supplementary Materials: The following are available online at <https://www.mdpi.com/article/10.3390/rs14132974/s1>, Figure S1: The relative spectral response of the ZWO ASI1600MM-Cool camera, employed in the Maceió recordings, Figure S2: The original first frame of detection of Flash 1, as recorded in Maceió, non-cropped, representing the effective FOV of the setup that was used in the site, Figure S3: TIFF file generated by LunarScan for the frame with the peak of Flash 1, from the Maceió recordings. Inverted colors, Figure S4: TIFF file generated by LunarScan for the frame with the peak of Flash 1, from the Araruna recordings. Inverted colors. The black spot is the flash. The white dots are hot pixels, Figure S5: TIFF file generated by LunarScan for the frame with the peak of Flash 2, from the Maceió recordings. Inverted colors, Figure S6: TIFF file of seven-frame sequence generated by LunarScan for Flash 2, from the recordings at Maceió, at 4.46 FPS, Figure S7: Reported ZHR of the Geminid meteor shower around its 2017 peak, according to the IMO.

Author Contributions: Conceptualization, D.D.C.P. and M.Y.; methodology, D.D.C.P., M.Y. and M.L.d.P.V.Z.; investigation, D.D.C.P., M.Y. and M.L.d.P.V.Z.; software, D.D.C.P., M.L.d.P.V.Z., M.Y., R.L.d.R.J., L.d.M.T., E.R.d.S.J. and N.D.C.J.; validation, M.Y., D.D.C.P., R.L.d.R.J., R.L.C., F.D.d.S.S., H.B.G. (Heliofábio Barros Gomes) and H.B.G. (Helber Barros Gomes); formal analysis, M.Y., D.D.C.P., M.L.d.P.V.Z. and R.L.d.R.J.; data curation, D.D.C.P., M.L.d.P.V.Z., R.A.A.C., L.d.M.T., E.R.d.S.J. and N.D.C.J.; writing—original draft preparation, D.D.C.P., M.Y. and M.L.d.P.V.Z.; writing—review and editing, D.D.C.P., M.Y., F.D.d.S.S. and M.L.d.d.M.; visualization, M.Y., D.D.C.P., M.L.d.P.V.Z., F.D.d.S.S., R.L.C., R.A.A.C., M.D., L.d.M.T., E.R.d.S.J., N.D.C.J. and H.B.G. (Helber Barros Gomes); supervision, D.D.C.P. and M.Y.; project administration, D.D.C.P.; resources, R.A.A.C., M.L.d.P.V.Z. and M.D.; funding acquisition, F.D.d.S.S., M.Y., D.L.H., R.L.C., M.L.d.d.M., H.B.G. (Helber Barros Gomes) and H.B.G. (Heliofábio Barros Gomes). All authors have read and agreed to the published version of the manuscript.

Funding: The APC was funded by the Programa de Apoio à Pós-Graduação (PROAP), of the Coordination for the Improvement of Higher Education Personnel (CAPES).

Institutional Review Board Statement: Not applicable.

Informed Consent Statement: Not applicable.

Acknowledgments: We thank CAPES for the financial support provided through their PROAP program, as well as the anonymous reviewers for their impressively meticulous considerations, which resulted in ample improvements to our paper. Furthermore, we would like to thank most especially Masahisa Yanagisawa, whose continued dedication to science is an inspiration to us all.

Conflicts of Interest: The authors declare no conflict of interest.

References

1. Oberst, J.; Christou, A.; Suggs, R.; Moser, D.; Daubar, I.J.; McEwen, A.S.; Burchell, M.; Kawamura, T.; Hiesinger, H.; Wünnemann, K.; et al. The present-day flux of large meteoroids on the lunar surface—A synthesis of models and observational techniques. *Planet. Space Sci.* **2012**, *74*, 179–193. [\[CrossRef\]](#)
2. Yanagisawa, M.; Ohnishi, K.; Takamura, Y.; Masuda, H.; Sakai, Y.; Ida, M.; Adachi, M.; Ishida, M. The first confirmed Perseid lunar impact flash. *Icarus* **2006**, *182*, 489–495. [\[CrossRef\]](#)
3. Avdellidou, C.; Munaibari, E.; Larson, R.; Vaubaillon, J.; Delbo, M.; Hayne, P.; Wieczorek, M.; Sheward, D.; Cook, A. Impacts on the Moon: Analysis methods and size distribution of impactors. *Planet. Space Sci.* **2021**, *200*, 105201. [\[CrossRef\]](#)
4. Anderson, B.J. *Natural Orbital Environment Guidelines for Use in Aerospace Vehicle Development*; NASA Technical Memorandum 4527; NASA Marshall Space Flight Center: Huntsville, AL, USA, 1994.
5. McNamara, H.; Suggs, R.; Kauffman, B.; Jones, J.; Cooke, W.; Smith, S. Meteoroid Engineering Model (MEM): A Meteoroid Model for The Inner Solar System. In *Modern Meteor Science an Interdisciplinary View*; Springer: Dordrecht, The Netherlands, 2004; Volume 95, pp. 123–139. [\[CrossRef\]](#)
6. Ortiz, J.L.; Aceituno, F.J.; Aceituno, J. A search for meteoritic flashes on the Moon. *Astron. Astrophys.* **1999**, *343*, L57–L60.
7. Dunham, D.W.; Cudnik, B.; Palmer, D.M.; Sada, P.V.; Melosh, J.; Beech, M.; Pellerin, L.; Asher, D.; Frankenberger, R.; Venable, R. The first confirmed videorecordings of lunar meteor impacts. *Lunar Planet. Sci.* **2000**, XXXI, 1547.

8. Ortiz, J.L.; Sada, P.V.; Bellot Rubio, L.R.; Aceituno, F.J.; Aceituno, J.; Gutierrez, P.J.; Thiele, U. Optical detection of meteoroidal impacts on the Moon. *Nature* **2000**, *405*, 921–923. [\[CrossRef\]](#) [\[PubMed\]](#)
9. Yanagisawa, M.; Kisaichi, N. Lightcurves of 1999 Leonid impact flashes on the Moon. *Icarus* **2002**, *159*, 31–38. [\[CrossRef\]](#)
10. Suggs, R.M.; Moser, D.E.; Cooke, W.J.; Suggs, R.J. The flux of kilogram-sized meteoroids from lunar impact monitoring. *Icarus* **2014**, *238*, 23–26. [\[CrossRef\]](#)
11. Madieto, J.M.; Ortiz, J.L.; Yanagisawa, M.; Aceituno, J.; Aceituno, F. Impact flashes of meteoroids on the moon. In *Meteoroids: Sources of Meteors on Earth and Beyond*; Ryabova, G.O., Asher, D.J., Campbell-Brown, M.D., Eds.; Cambridge University Press: Cambridge, UK, 2019; pp. 136–158. [\[CrossRef\]](#)
12. Liakos, A.; Bonanos, A.Z.; Xilouris, E.M.; Koschny, D.; Bellas-Velidis, I.; Boumis, P.; Charmandaris, V.; Dapergolas, A.; Fytisilis, A.; Maroussis, A. NELIOTA: Methods, statistics, and results for meteoroids impacting the moon. *Astron. Astrophys.* **2020**, *633*, A112. [\[CrossRef\]](#)
13. Yanagisawa, M.; Uchida, Y.; Kurihara, S.; Abe, S.; Fuse, R.; Tanaka, S.; Onodera, K.; Yoshida, F.; Chi, H.C.; Lin, Z.Y.; et al. Low dispersion spectra of lunar impact flashes in 2018 Geminids. *Planet. Space Sci.* **2021**, *195*, 105131. [\[CrossRef\]](#)
14. Melosh, H.J. *Impact Cratering: A Geologic Process*; Oxford University Press: New York, NY, USA, 1989. [\[CrossRef\]](#)
15. Burchell, M.J.; Cole, M.J.; Ratcliff, P.R. Light Flash and Ionization from Hypervelocity Impacts on Ice. *Icarus* **1996**, *122*, 359–365. [\[CrossRef\]](#)
16. Burchell, M.J.; Kay, L.; Ratcliff, P.R. Use of combined light flash and plasma measurements to study hypervelocity impact processes. *Adv. Space Res.* **1996**, *17*, 141–145. [\[CrossRef\]](#)
17. Bouley, S.; Baratoux, D.; Vaubaillon, J.; Mocquet, A.; Le Feuvre, M.; Colas, F.; Benkhaldoun, Z.; Daassou, A.; Sabil, M.; Lognonné, P. Power and duration of impact flashes on the Moon: Implication for the cause of radiation. *Icarus* **2012**, *218*, 115–124. [\[CrossRef\]](#)
18. Rembold, J.J.; Ryan, E.V. Characterization and Analysis of Near-Earth Objects via Lunar Impact Observations. *Planet. Space Sci.* **2015**, *117*, 119–126. [\[CrossRef\]](#)
19. Madieto, J.M.; Ortiz, J.L.; Morales, N.; Cabrera-Caño, J. A large lunar impact blast on 2013 September 11. *Mon. Not. R. Astron. Soc.* **2014**, *439*, 2364–2369. [\[CrossRef\]](#)
20. Suggs, R.M.; Ehlert, S.R.; Moser, D.E. A comparison of radiometric calibration techniques for lunar impact flashes. *Planet. Space Sci.* **2017**, *143*, 225–229. [\[CrossRef\]](#)
21. Cudnik, B.M.; Dunham, D.W.; Palmer, D.M.; Cook, A.; Venable, R.; Gural, P.S. The Observation and Characterization of Lunar Meteoroid Impact Phenomena. *Earth Moon Planets* **2003**, *93*, 97–106. [\[CrossRef\]](#)
22. Yamada, R.; Garcia, R.F.; Lognonné, P.; Le Feuvre, M.; Calvet, M.; Gagnepain-Beyneix, J. Optimisation of seismic network design: Application to a geophysical international lunar network. *Planet. Space Sci.* **2011**, *59*, 343–354. [\[CrossRef\]](#)
23. Larbi, M.A.M.; Daassou, A.; Baratoux, D.; Bouley, S.; Benkhaldoun, Z.; Lazrek, M.; Garcia, R.; Colas, F. First Lunar Flashes Observed from Morocco (ILIAD Network): Implications for Lunar Seismology. *Earth Moon Planets* **2015**, *115*, 1–21. [\[CrossRef\]](#)
24. Nakamura, Y.; Latham, G.V.; Dorman, H.J.; Harris, J.E. *Passive Seismic Experiment Long Period Event Catalog, Final Version*; UTIG Technical Report No. 18; Institute for Geophysics: Austin, TX, USA, 1981.
25. Lognonné, P.; Le Feuvre, M.; Johnson, C.L.; Weber, R.C. Moon meteoritic seismic hum: Steady state prediction. *J. Geophys. Res.* **2009**, *114*, E12. [\[CrossRef\]](#)
26. Sheward, D.; Cook, A.; Avdellidou, C.; Delbo, M.; Cantarella, B.; Zanatta, L.; Sposetti, S.; Lena, R. Lunar Surface Change Detection with PyNAPLE: The 2017-09-27 Lunar Impact Flash and Impact Crater. *Euro-Planet Sci. Congr.* **2021**, *15*, EPSC2021-590. Available online: <https://meetingorganizer.copernicus.org/EPSC2021/EPSC2021-590.html> (accessed on 25 November 2021).
27. Babadzhinov, P.B.; Kokhirova, G.I. Densities and porosities of meteoroids. *Astron. Astrophys.* **2009**, *495*, 353–358. [\[CrossRef\]](#)
28. Kasuga, T.; Jewitt, D. Asteroid-meteoroid complexes. In *Meteoroids*; Ryabova, G.O., Asher, D.J., Campbell-Brown, M.D., Eds.; Cambridge University Press: Cambridge, UK, 2019; pp. 187–209. [\[CrossRef\]](#)
29. Abe, S.; Ogawa, T.; Maeda, K.; Arai, T. Sodium variation in Geminid meteoroids from (3200) Phaethon. *Planet. Space Sci.* **2020**, *194*, 105040. [\[CrossRef\]](#)
30. Vaubaillon, J.; Neslusan, L.; Sekhar, A.; Rudawska, R.; Ryabova, G.O. From parent body to meteor shower: The dynamics of meteoroid streams. In *Meteoroids*; Ryabova, G.O., Asher, D.J., Campbell-Brown, M.D., Eds.; Cambridge University Press: Cambridge, UK, 2019; pp. 161–186. [\[CrossRef\]](#)
31. Jewitt, D.; Hsieh, H.; Agarwal, J. The active asteroids. In *Asteroids IV*; Michel, P., De Meo, F.E., Bottke, W.F., Eds.; University Arizona Press: Tucson, AZ, USA, 2015; pp. 221–241. [\[CrossRef\]](#)
32. Ryabova, G.O. The mass of the Geminid meteoroid stream. *Planet. Space Sci.* **2017**, *143*, 125–131. [\[CrossRef\]](#)
33. Madieto, J.M.; Ortiz, J.L.; Morales, N.; Cabrera-Caño, J. MIDAS: Software for the detection and analysis of lunar impact flashes. *Planet. Space Sci.* **2015**, *111*, 105–115. [\[CrossRef\]](#)
34. Ortiz, J.L.; Madieto, J.M.; Morales, N.; Santos-Sanz, P.; Aceituno, F.J. Lunar impact flashes from Geminids: Analysis of luminous efficiencies and the flux of large meteoroids on Earth. *Mon. Not. R. Astron. Soc.* **2015**, *454*, 344–352. [\[CrossRef\]](#)
35. Nemtchinov, I.V.; Shuvalov, V.V.; Artemieva, N.A.; Ivanov, B.A.; Kosarev, I.B.; Trubetskaya, I.A. Light flashes caused by impacts against the moon. In *AIP Conference Proceedings, Proceedings of The Tenth American Physical Society Topical Conference on Shock Compression of Condensed Matter, Amherst, MA, USA, 27 July–1 August 1997*; Schmidt, S.C., Dandekar, D.P., Forbes, J.W., Eds.; American Institute of Physics: College Park, MD, USA, 1998; Volume 429, pp. 957–962. [\[CrossRef\]](#)

-
36. Kim, E.; Kim, Y.H.; Hong, I.-S.; Yu, J.; Lee, E.; Kim, K. Detection of an Impact Flash Candidate on the Moon with an Educational Telescope System. *J. Astron. Space Sci.* **2015**, *32*, 121–125. [[CrossRef](#)]
 37. Madiedo, J.M.; Ortiz, J.L.; Organero, F.; Ana-Hernández, L.; Fonseca, F.; Morales, N.; Cabrera-Caño, J. Analysis of Moon impact flashes detected during the 2012 and 2013 Perseids. *Astron. Astrophys.* **2015**, *577*, A118. [[CrossRef](#)]
 38. Flower, P.J. Transformations from theoretical Hertzsprung-Russell diagrams to color-magnitude diagrams: Effective temperatures, B-V colors, and bolometric corrections. *Astrophys. J.* **1996**, *469*, 355–365. [[CrossRef](#)]
 39. Bessell, M.S. Standard photometric systems. *Annu. Rev. Astron. Astrophys.* **2005**, *43*, 293–336. [[CrossRef](#)]
 40. Gray, D. Background. In *The Observation and Analysis of Stellar Photospheres*; Cambridge University Press: Cambridge, UK, 2005; pp. 1–25. [[CrossRef](#)]
 41. Schubert, G.; Walterscheid, R.L. Earth. In *Allen's Astrophysical Quantities*, 4th ed.; Cox, A.N., Ed.; Springer: New York, NY, USA, 1999; pp. 239–292.
 42. Bellot Rubio, L.R.; Ortiz, J.L.; Sada, P.V. Luminous efficiency in hypervelocity impacts from the 1999 Lunar Leonids. *Astrophys. J.* **2000**, *542*, L65–L68. [[CrossRef](#)]
 43. Bellot Rubio, L.R.; Ortiz, J.L.; Sada, P.V. Observation and interpretation of meteoroid impact flashes on the Moon, 1998 for the online version. *Earth Moon Planets* **2000**, *82–83*, 575–598. [[CrossRef](#)]
 44. Babadzhanov, P.B. Fragmentation and densities of meteoroids. *Astron. Astrophys.* **2002**, *384*, 317–321. [[CrossRef](#)]
 45. Gault, D.E. Impact cratering. In *A Primer in Lunar Geology*; Ames Research Center: Moffett Field, CA, USA, 1974; pp. 137–175.
 46. McKay, D.S.; Heiken, G.; Basu, A.; Blanford, G.; Simon, S.; Reedy, R.; French, B.M.; Papike, J. The lunar regolith. In *Lunar Source Book*; Heiken, G.H., Vaniman, D.T., French, B.M., Eds.; Cambridge University Press: Cambridge, UK, 1991; pp. 285–356.